UNIVERSITY *of* York

This is a repository copy of *Design Method for Variable Frequency Brushless Synchronous Generators*.

White Rose
university consortium
Universities of Leeds, Sheffield & York

eprints@whiterose.ac.uk
https://eprints.whiterose.ac.uk/

Article

Design Method for Variable Frequency Brushless Synchronous Generators

Yongjie Wang [1],*, Huizhen Wang [1], Weifeng Liu [1], Qin Wang [1] and Xing Zhao [2]

1. Center for More-Electric-Aircraft Power Systems, Nanjing University of Aeronautics and Astronautics, Nanjing 211006, China; Wanghz@nuaa.edu.cn (H.W.); 15150654203@139.com (W.L.); wangqin@nuaa.edu.cn (Q.W.)
2. Department of Electronic Engineering, University of York, York YO10 5DD, UK; xing.zhao@york.ac.uk
* Correspondence: wyj@nuaa.edu.cn

Abstract: Brushless synchronous generators, which have the structure of three-stage generators to realize brushless excitation, are the most commonly used aero-generators. With the development of more electric aircraft technology, the output frequency of aero-generators is changing from constant to variable, and the characteristics of generators are also changed. To make sure that the generators can be adapted to the variable frequency operation, this paper analyzes the effects of different operating conditions on generator performance and proposes corresponding design methods. The design and verification of the electromagnetic field, fluid field, temperature field and stress field are carried out for the variable frequency generator. A prototype generator is manufactured according to the design results. An experimental platform is set up to test the performances of the designed generator. The final experimental results show that the generator can work well in variable frequency generation systems, which proves the design method proposed in this paper is effective and feasible.

1. Introduction

Since the beginning of the 21st century, more electric aircraft (MEA) technology has been widely applied, aiming to replace part of the aircraft's secondary energy system with the electrical system, most of the onboard equipment are powered by electrical energy. MEA technology can effectively improve aircraft reliability and maintainability, reduce operating costs and the weight of the aircraft [1–3].

At present, civil airliners with MEA technology features mainly include Airbus' A380, A350XWB and Boeing's B787. The most important feature of these aircrafts is the replacement of the original Integrated Drive Generator (IDG) with a variable frequency generator (VFG). Table 1, below, shows the generator data of several wide-body aircraft. The generators before 2000 are in the range of 90 kVA to 120 kVA. The frequency of the output voltages is fixed to 400 Hz. The generators of MEAs are changed from IDG to VFG, the capacities are increased to the range of 100 kVA to 250 kVA. At the same time, the voltage level of the A350 and B787 are both doubled, thus the losses and weights of the cables can be reduced.

IDG is a kind of generator that integrates constant speed drive (CSD) and brushless synchronous generator (BSG). The constant speed operation of the generator is realized by CSD, which results in the output of alternating current with a constant 400 Hz frequency. Table 2 lists the weight data of several IDGs; it can be found that the weight of CSD generally accounts for about 60% to 70% of the total weight of IDG, which seriously restricts the power density of aero-generators.

Table 1. Typical wide-body passenger aircraft power system capacity data [4].

Type	Twin-Engine Jet				Four-Engine Jet	
Aircraft	A330	B777	B787	A350	B747	A380
First flight year	1992	1994	2009	2013	1988	2005
Rated voltage/V	115	115	230	230	115	115
Number of generators	2	2	4	4	4	4
Rated capacity/kVA	115	120	250	100	90	150
Generator type	IDG	IDG	VFG	VFG	IDG	VFG

Table 2. IDG's weight data comparison [5].

Aircraft	Rated Power	CSD Weight	IDG Weight	CSD Weight Share
A-10A	30/40 kVA	20.9 kg	34.5 kg	69.7%
F-14A	60/75 kVA	31.3 kg	51.7 kg	60.5%
F-15	40/50 kVA	22.2 kg	38.6 kg	57.5%
F-16	40 kVA	22.2 kg	37.6 kg	59.0%
B747	90 kVA	41.7 kg	62.6 kg	66.6%

In addition, the power density of the generator section is also affected by the need for a constant frequency. The rotor speed and pole pairs of the synchronous generator are constrained by the output voltage frequency, so increasing the rotor speed requires a corresponding decrease in the number of pole pairs. Therefore, in the 400 Hz constant generation system, the maximum generator speed is 24,000 rpm, which corresponds to 1 pole pair synchronous generator, so the increase in generator power density is limited [4].

The variable frequency generator eliminates the CSD and removes the frequency constraint, thus allowing for higher power density and greater generation capacity. However, compared to IDG, the operating frequency of VFG varies in the range of 360–800 Hz [6–8], the generator performance varies with the speed and frequency, which increases the difficulties of the generator design [9,10].

There are usually two methods to the design an aero-generator. The first method is to the optimization design based on the original generator [11]. In those cases, the electromagnetic load, current density and rotor stress can be easily selected based on the performance of the original generator. Another method is that when there is no original generator for reference, it is necessary to explore the verification of the working limit of the generator [12]. This means involving the calculation of multi-physical fields calculations, which includes electromagnetic field, fluid field, temperature field and stress field. While the working conditions of VSVF generator are far more than others, which leads to more calculations required in the design process. Therefore, for the design of VSCF generator, it is necessary to analyze the influence of different working conditions on its performance in advance, sort out the relationship and analyze and obtain the working conditions when various performances reach their limit values, so as to reduce the amount of relevant calculation and improve the design efficiency.

Literature [13–16] have studied the design method of aero-generator applied to high voltage direct current (HVDC) systems, but they only involve the design method of electromagnetic performance, lacks the content related to multi-physical fields. The authors of [17] proposed the electromagnetic, mechanical and thermal models of the aero-generator. These models are based on the analytical formula and are relatively simple. They are used to evaluate the impact of key dimensional parameters such as the length diameter ratio on the overall performance of the generator. The three-dimensional lumped parameter thermal network model of generator is proposed in literature [18], which lays a foundation for the multi-physical field design of aero-generators. Referring to the generator applied

in B787, the authors of [9] designed a generator with the same index, and simulated and verified the electromagnetic field, stress field, temperature field and other physical fields. The results show that the designed prototype can further improve the power density by replacing air cooling method with liquid cooling method.

It can be seen from the above literature that with the development of MEA technology, the design requirements of brushless synchronous generator are gradually improving, and the research on its multi-physical field design method is paid attention to by researchers.

In this paper, the influence of different operating conditions on the performance of BSGs is analyzed. The design method is proposed based on the previous analysis. The design and verification are implemented based on the electromagnetic field, fluid field, temperature field and stress field analysis. A prototype generator is manufactured and tested in an experimental platform. The performances of the designed generator operating at variable frequency are demonstrated in the last section.

2. Influence of the Operating Conditions

BSG consists of three stages: main generator (MG), exciter and permanent magnet generator (PMG) [8,19]. It is the most commonly used aero-generator because the brushless excitation is achieved by the application of the exciter, which improves the service life of the synchronous generators. The complete BSG system structure is shown in Figure 1.
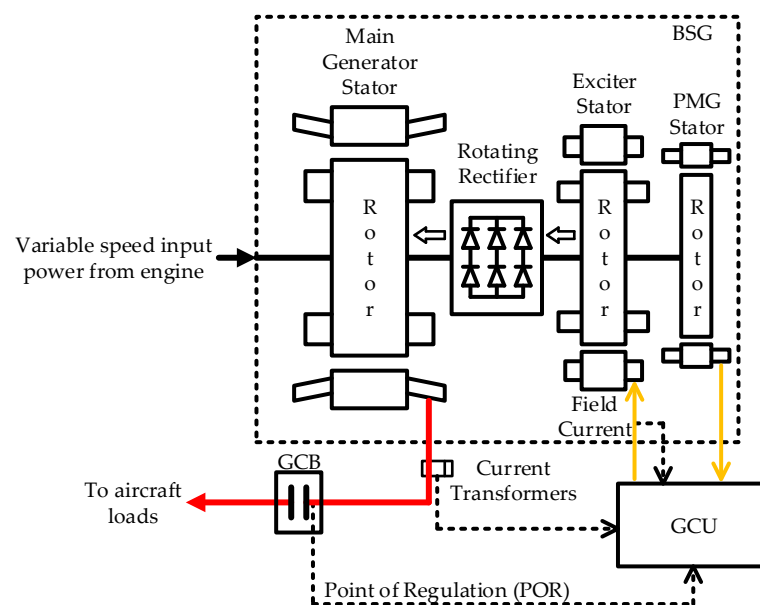

Figure 1. BSG system schematic.

The design requirements of BSGs are mainly divided into three kinds: electromagnetic performance, mechanical performance and cooling performance: the electromagnetic performance requirements include rated voltage, rated power, rated frequency, power factor, efficiency, overload capacity and power quality; the mechanical performance requirements include generator weight, volume size, rated speed, maximum over-speed and static suspension moment; the cooling performance requirements include the cooling method and cooling medium. For example, the performance requirements of an emergency generator used for Ram Air Turbine (RAT) are shown in Table 3, where the items 1–7 are electromagnetic performance requirements, items 8–12 are mechanical performance requirements and the item 13nis the cooling performance requirements.

Table 3. Generator performance requirements.

No.	Performance Items	Unit	Performance Indicators
1	Rated voltage	Vrms	230/400
2	Power rating	kVA	10
3	Rated frequency	Hz	453~641
4	Power factor		0.75 (lag.) to 1.00
5	Efficiency		$\not< 80\%$
6	Overload capacity	kVA	15 (last 5 min) 20 (last 5 s)
7	Electricity quality		MIL-STD-704F
8	Weight	kg	$\not> 40$
9	Size	mm	$\not> 600 \times 600 \times 600$
10	Rated speed	rpm	6795~9615
11	Maximum overspeed	rpm	10,000 (last 5 min)
12	Static suspension torque	N·m	$\not> 100$
13	Cooling method		Forced air cooling

The power quality requirements of generators include voltage accuracy, crest factor, voltage modulation amplitude, voltage phase difference, distortion factor, harmonic content and distortion spectrum. These indicators are usually determined by the electromagnetic design of the MG.

The impact of different operating conditions on generator performance varies. The influences of flight altitude, temperature, rotor speed and load conditions, on the generator performance, are as follows.

(1) Flight altitude

The flight altitude of military helicopters is generally 3000 to 6000 m, civil airliners are generally 10,000 to 13,000 m, and the fighters are 18,000 to 20,000 m. Accordingly, the onboard equipment needs to adapt to the change in flight altitude. When the altitude rises from 0 to 20,000 m, the atmospheric pressure decreases by 94.6%, the air temperature decreases by 71.5 °C, the air density and the specific heat capacity of air volume decrease by 92.8%. The flight altitude is higher, the air becomes thinner. Although the friction loss of the generator will be significantly reduced at this time, the cooling capacity of the air-cooled system decreases sharply.

(2) Temperature

According to DO-160G, aero-generators need to adapt to the ambient temperature of −55 to 70 °C. Different ambient temperatures affect the physical properties of electromagnetic materials and cooling media. At the same time, the losses generated by the generator in the process of power generation will also be converted into heat, affecting the temperature of the motor components.

To increase the power density of the generator, the winding of the generator is usually selected as C-class insulation material, which can withstand temperatures of 200 to 240 °C. Therefore, the temperature of the generator winding will vary between −60 and 180 °C. When the temperature of the winding becomes higher, the changes in the generator performances are as follows:

(a) The armature winding temperature rise leads to an increase in voltage drop, resulting in more excitation power requirements.

(b) The winding temperature rise leads to higher winding resistance, increased copper losses and lower efficiency.

(c) The resistance of dumping windings becomes larger, the negative sequence impedance increases and the generator performances under unbalanced loads become poorer.

(d)   The rotating rectifier operating mode is affected by the winding temperature.
(e)   The performance of permanent magnets in PMG decreases and the risk of demagnetization is greater.

(3) Rotor speed

Compared with IDG, VFG needs to meet the performance requirements at different rotor speeds, which will affect the magnetic saturation characteristics of the generator and change the reactance, thus affecting the generator performance. The specific impact includes the following aspects:

(a)   The speed is higher, the core saturation is less and less excitation power is required.
(b)   The skin effect and proximity effect of the generator windings will be more obvious with the increase in frequency, so the AC loss is greater.
(c)   Eddy current losses in the damping windings of the main generator and the permanent magnets of the PM machine become larger as the frequency increases.
(d)   High speed corresponds to high frequency, the reactance of the generator becomes larger, the armature reaction is enhanced.
(e)   Variations in the MG excitation current and the armature reactance of the exciter also affect the rectifier operating mode of the rotation rectifier.
(f)   The stress of the generator rotor will be greater under the higher speed, which will increase the risk of structural damage to the generator rotor.

(4) Load conditions

Aero-generators need to work under different load conditions. Not only the output power but also the power factor changes. At the same output power, the armature reaction of the MG under inductive load will be greater compared to the resistive load, so the generator needs more excitation power when the power factor becomes smaller.

In addition, generators need to have a certain overload capacity and short-circuit capability, these variable load conditions can also have impact on the electromagnetic performances.

A comprehensive analysis of the impact of the above operating conditions on the performance of generators can be summarized as the following operating conditions that need to be considered in the design process of generators.

(a)   The power capability of the generator needs to be checked at high temperature and low-speed conditions.
(b)   The magnetic circuit saturation of the generator needs to be checked under high temperature, low speed and inductive overload conditions.
(c)   The power quality of the generator needs to be checked under high temperature and high-speed conditions, the load conditions depend on the specific situation.
(d)   The electromagnetic losses of the generator reach their maximum values at high temperature, low speed and inductive overload conditions.
(e)   The winding temperature rise of the generator needs to be checked at high flight altitude, high temperature, low speed and inductive overload conditions.
(f)   The structural strength of the generator rotor needs to be checked under high temperature and high-speed conditions.

3. Design Method

Based on the previous analysis, the generator has variable operating conditions and performance requirements, which requires the designers to adopt a multi-physics field design approach in the design process [20]. The complete design process of a generator consists of three parts: electromagnetic design, cooling design and structural design.

The design of exciter and PMG depend on the excitation power of MG and exciter respectively, so it is necessary to design the MG first, then the exciter and finally the PMG, the design process is shown in Figure 2.
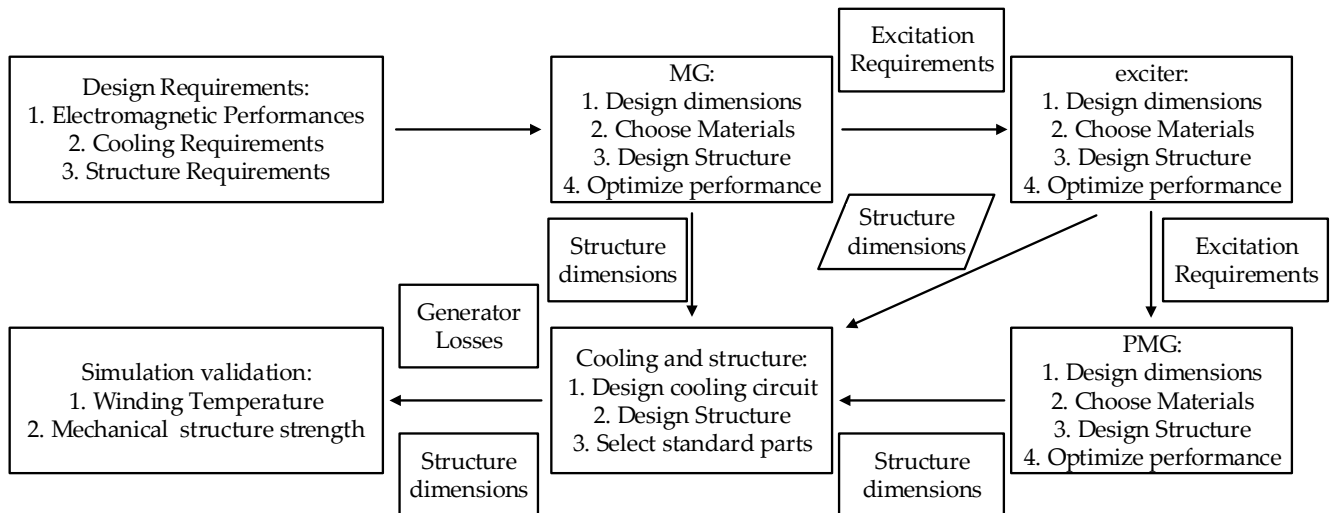

Figure 2. The flow chart of the BSG design process.

3.1. Electromagnetic Design

The effective material weight of the MG usually accounts for 50% to 70% of the total weight of the BSG. Take a JF-10D generator as an example, the total weight of the generator is 8.5 kg and the effective material weight of the stator/rotor of the main generator is 2.78 kg and 1.47 kg respectively, the effective material weight of the MG is exactly 50% of the total weight of the generator, as shown in Figure 3. Therefore, the effective material weight of the MG can be set as 50% of the total weight of the generator during the design process.
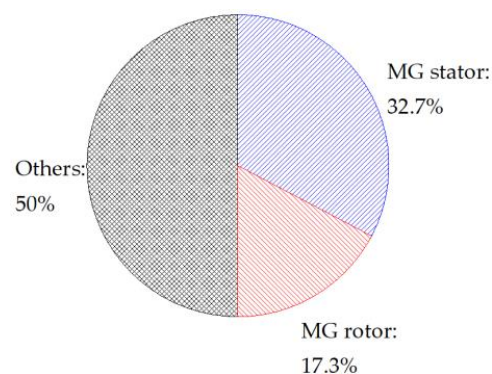

Figure 3. JF-10D generator weight distribution diagram.

The conventional electromagnetic design process of the MG is shown in Figure 4. The related formula calculation can be found in the literature [21].
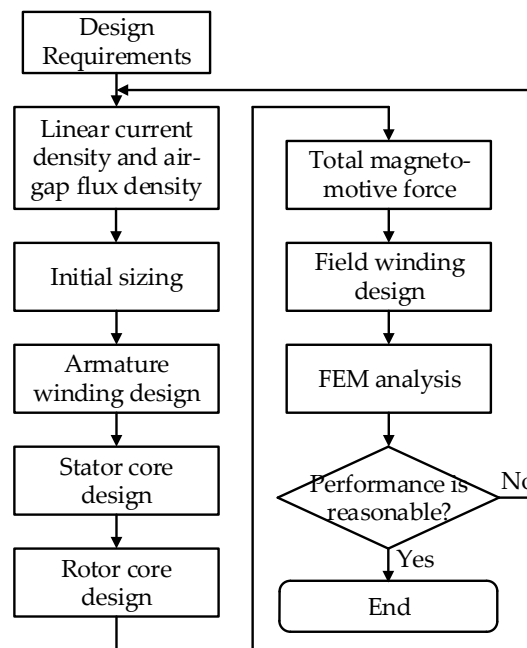
Figure 4. Schematic diagram of the conventional main generator electromagnetic design flow.

For variable frequency BSGs, the power quality requirements are more difficult to meet under high-speed conditions, so extra attention is needed in the electromagnetic design process. The most important power quality requirements are the harmonic content of the output voltage and the voltage unbalance and phase shift under the unbalanced load, the latter determined by the MG's negative sequence impedance [22]. There are three main influencing factors, which are analyzed in detail as follows.
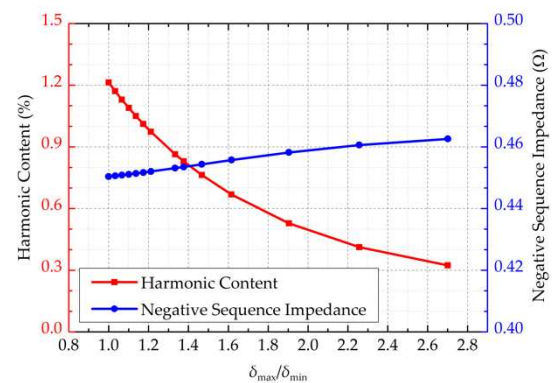
(1) Air gap

The air gap shape parameters mainly include armature slot opening B_{s0}, air gap length δ and pole arc coefficient α_p, their effects on generator voltage harmonic content and negative sequence impedance are shown in Figure 5. According to the data in the figure, it is known that:

(a)   When the B_{s0} becomes greater, the negative sequence impedance decreases sharply and the harmonic content decreases slightly.

(b)   The more uneven the air gap is, the smaller the harmonic content is.

(c) α_p has a limited influence on the negative sequence impedance, but its effect on the harmonic content is significant, as α_p gradually increases, the harmonic content first increases and then decreases.
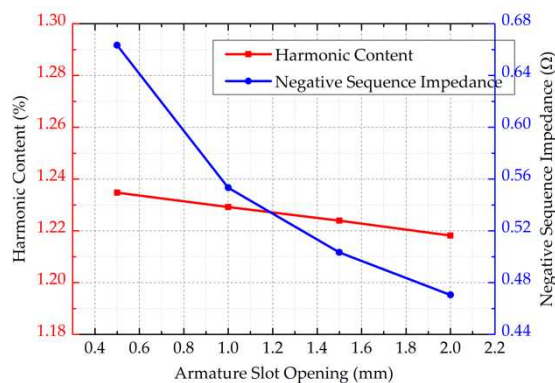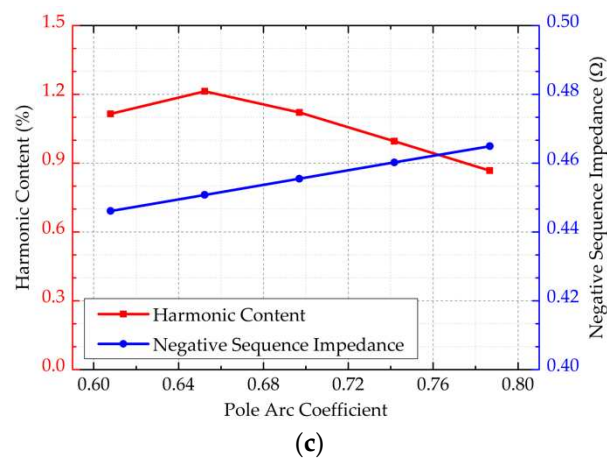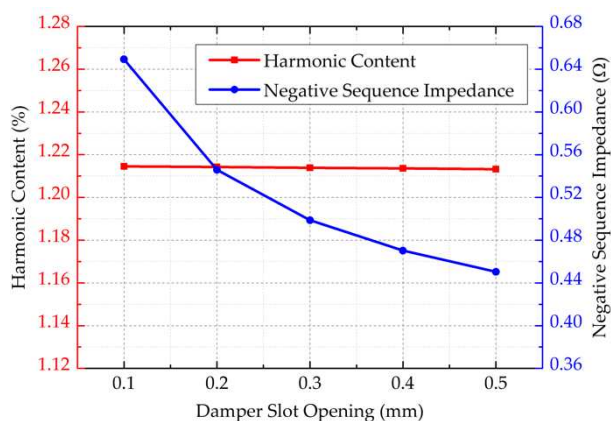

(**a**)

(**b**)

Figure 5. *Cont.*

Figure 5. Harmonic content and negative sequence impedance variation curve with air gap size parameters: (**a**) Effect of armature slot opening; (**b**) Effect of air gap length; (**c**) Effect of polar arc coefficient.
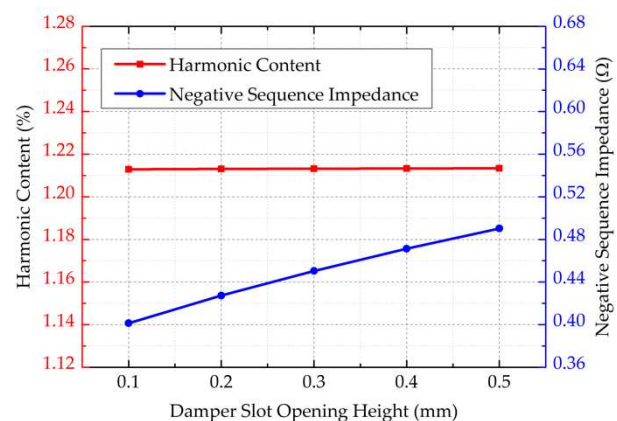
(2) Damping winding

The damping winding parameters mainly include damper slot opening B_{d0}, damper slot opening height H_{d0}, damper diameter D_d and damper slot pitch SP, their effects on generator voltage harmonic content and negative sequence impedance are shown in Figure 6. According to the data in the figure, it can be seen that:

(a)　The parameters related to the damping winding have an almost slight effect on the harmonic content and are mainly used to reduce the negative sequence impedance.

(b)　The negative sequence impedance decreases significantly with the increase of B_{d0}.

(c)　H_{d0} has a greater effect on the negative sequence impedance.

(d)　The influence of D_d on the negative sequence impedance is small. When D_b increases, although the negative sequence resistance decreases, the leakage reactance of the damping winding increases, which leads to a larger negative sequence impedance.

(e)　The effect of SP on the negative sequence impedance is small.
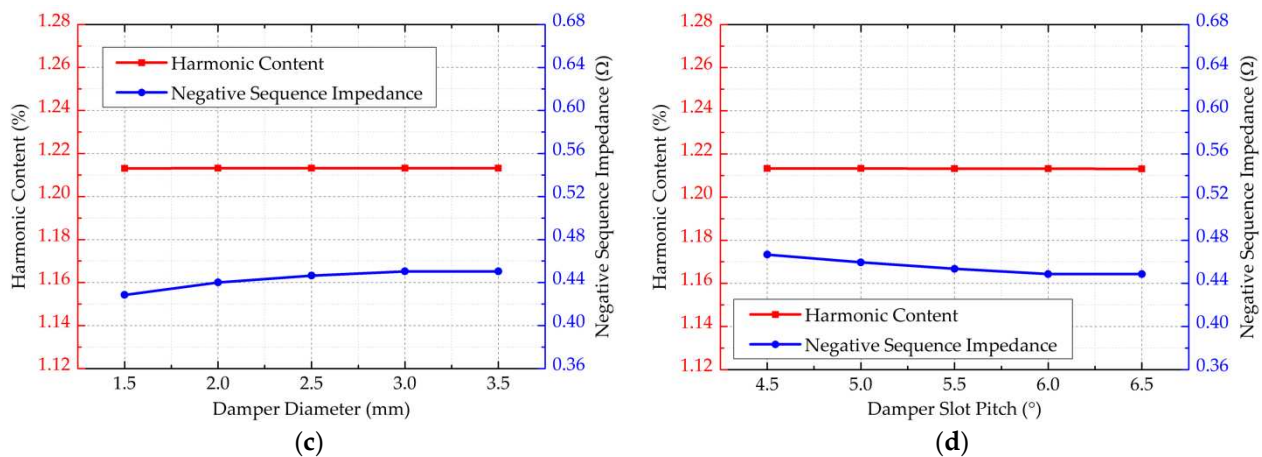

Figure 6. *Cont.*

Figure 6. Harmonic content and negative sequence impedance variation curve with damping winding parameters: (**a**) Effect of damper slot opening; (**b**) Effect of damper slot opening height; (**c**) Effect of damper diameter; (**d**) Effect of damper slot pitch.

(3) The turns of armature winding

Figure 7 shows the effect of turns-in-series per phase of the armature winding N_s on the harmonic content and negative sequence impedance, while the airgap flux density keeps constant. It can be found that N_s have a significant effect on both performances, and both become significantly larger as N_s increase.
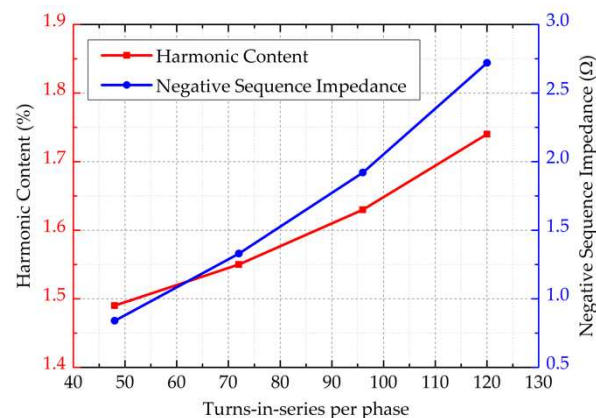

Figure 7. Harmonic content and negative sequence impedance variation curve with armature winding turn.

According to the previous analysis, in the electromagnetic design process of the MG, it is necessary to adjust the air gap shape according to the voltage harmonic content and to adjust the damping winding parameters according to the negative sequence impedance. If the two adjustments cannot meet the requirements, it is necessary to reduce the turns-in-series per phase, which means reducing the power density of the MG in exchange for the improvement of power quality.

According to the above analysis, in the VSVF systems, in order to design the main generator more reasonably, the design process should be divided into two parts, including the design of main dimensional parameters and the design of waveform performance. The proposed design method is shown in Figure 8.
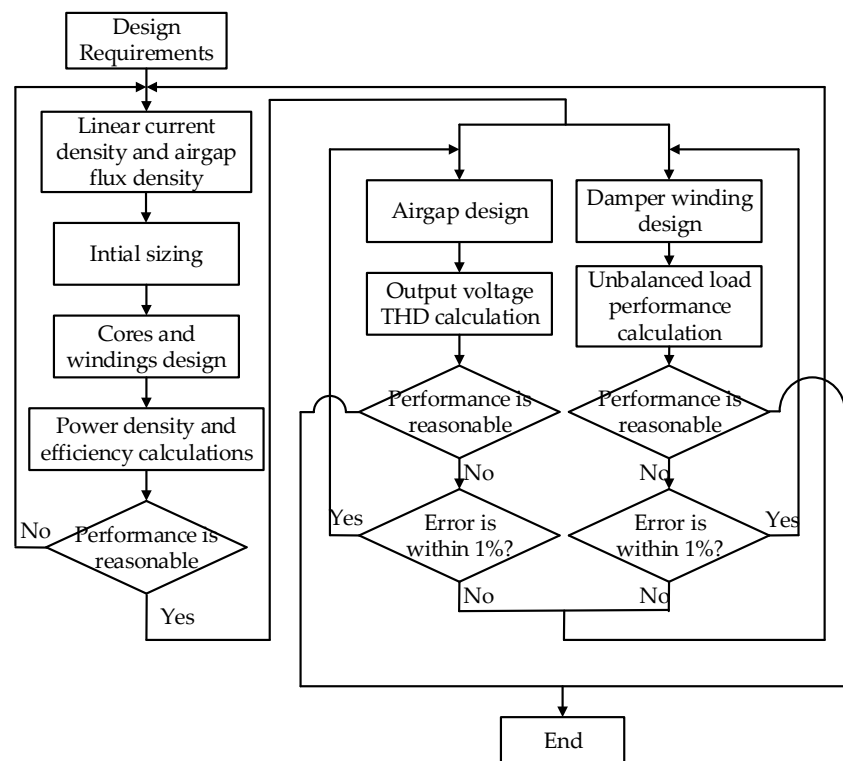
Figure 8. Proposed design method.

After the design of the MG is completed, its excitation data can be calculated by the Finite Element Method (FEM) simulation software, the optimization design of the exciter can be started. The exciter is a rotating-armature synchronous generator, whose electromagnetic design process is similar to that of the MG, but the performance requirements are completely different. In order to achieve the linear current amplifier characteristics of the generator, the exciter needs to reduce its air gap length, increase the number of winding turns and reserve sufficient margin for current overshoot during transients.

The PMG is also a synchronous generator, but the excitation winding is replaced with permanent magnets, so the design approach will be somewhat different. Due to the characteristics of permanent magnets, the PMG cannot be demagnetized in a short circuit fault, so their armature windings should be designed to high impedance to reduce the short circuit currents.

The parameters of the BSG obtained from the final design are shown in Table 4. Since this BSG is a technology verification prototype, the generator cores use silicon steel instead of iron–cobalt–vanadium alloy.

Table 4. RAT10k generator-related parameters.

No.	Parameters	Unit	MG	Exciter	PMG
1	Number of slots		60	30	12
2	Number of pole pairs		4	5	5
3	Core length	mm	145	12	9
4	Stator outer diameter	mm	186	186	70
5	Stator inner diameter	mm	150	148.8	50
6	Air gap length	mm	1.0	0.4	1.5
7	Rotor inner diameter	mm	64	110	34
8	Pole arc coefficient		0.65	0.72	0.9

Table 4. *Cont.*

| No.	Parameters	Unit	MG	Exciter	PMG
9	Armature winding turns		40	20	180
10	Armature winding strands		1	13	2
11	Armature winding size	mm	2.8×1.8	$\varnothing 0.63$	$\varnothing 0.45$
12	Excitation winding turns		14	58	-
13	Excitation winding strands		1	3	-
14	Excitation winding size	mm	6.3×1.4	$\varnothing 0.63$	-
15	Damping winding diameter	mm	3.0	-	-
16	Thickness of permanent magnets	mm	-	-	2
17	Effective material weight	kg	20.6	1.97	0.33

3.2. Cooling Design

According to the parameters of the designed generator, the loss data are obtained by the FEM simulation [23,24] as shown in Table 5, the generator is operating under 180 °C winding temperature, 6795 rpm, two times overload, 0.75 power factor. Based on these loss data, the design of the cooling system can be carried out.

Table 5. BSG loss data (unit: W).

| | Core Loss | Copper Loss | | | Rectifier Loss |
		Armature Winding	Excitation Winding	Damper Winding	
MG	280.11	245.47	506.69	28.16	-
Exciter	12.62	110.19	67.24	-	4.0

The BSG is axially ventilated and cooled, its internal air path is set up as shown in Figure 9, the red arrows indicate the direction of cooling air flow. The cooling airflow enters the BSG from the non-drive end cap, passes through the exciter and the rotating rectifier first, and then passes through the MG, and finally is pumped outside the drive end cap by the fan. The air paths of the exciter as well as the MG are 3-way parallel structure, passing through the stator, the air gap and the rotor, respectively. The fan is used for the ground testing.
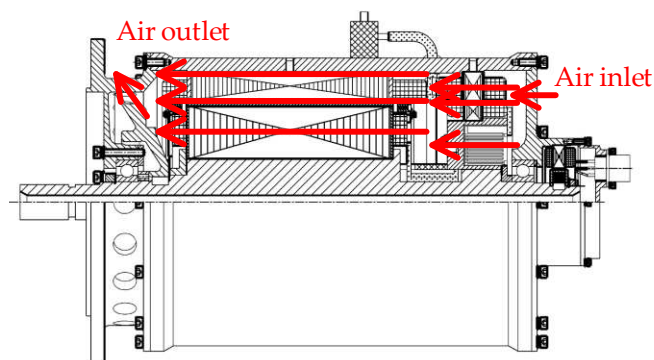
Figure 9. Schematic diagram of generator cooling air path structure.

In order to calculate the total ventilation resistance of the cooling circuit, it is necessary to simplify the flow-network structure and perform s eries/parallel equivalent calculations to obtain the total value. The calculation formula of ventilation resistance is [25]:

$$Z_n = \alpha_n \frac{\gamma}{2g} \frac{1}{S_n^2} \tag{1}$$

where α_n is the friction coefficient, γ is the specific gravity of air, g is the gravity acceleration, S_n is the cross-sectional area of the air path.

The value of the friction coefficient α_n is determined by the path structure. The air specific gravity γ can be calculated by the following equation:

$$\gamma = 0.0035 \frac{P_H}{273 + T_H} \tag{2}$$

where P_H is the air pressure at a specific altitude and T_H is the air temperature at a specific altitude.

It is known that the BSG's working altitude is from 0 m to 13,000 m, and the ambient temperature is from $-55\,°C$ to $70\,°C$, so the air resistance of the generator can be obtained as shown in the Table 6

Table 6. Ventilation resistance under different operating conditions (unit: $kg·s^2/m^6$).

	High Temperature (70 °C)	Low Temperature (−55 °C)
Sea level (0 m)	1922.33	3025.51
High altitude (13,000 m)	365.80	574.83

The ventilation resistance characteristic curve of the BSG can be calculated from the above table, as shown in Figure 10.
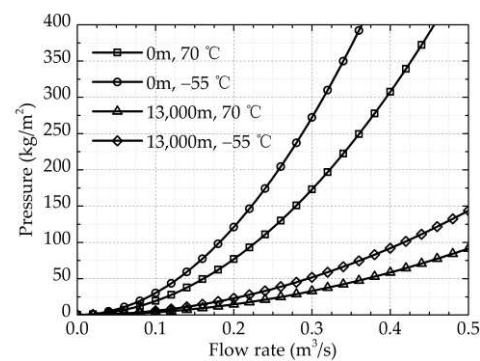

Figure 10. Ventilation resistance characteristics of the BSG.

The active pressure generated by the airflow during forced ventilation is

$$H = \frac{\gamma}{2g} v^2 \tag{3}$$

where v is the flight speed. This equation shows that the forced-air cooling system provides a fixed source of air pressure, which is related to the flight altitude, the ambient temperature and the flight speed.

Take B787 as an example, the lowest equivalent airspeed of its RAT at 13,000 m altitude is 180 KEAS, which is about 92.5 m/s; the lowest equivalent airspeed at sea level is 120 KEAS, which is about 62 m/s, so the air pressure data of forced-air cooling system can be obtained as shown in Table 7.

Table 7. Pressure generation under different operating conditions (unit: kg/m^2).

|	High Temperature (70 °C)	Low Temperature (−55 °C)
Sea level (0 m)	202.64	318.83
High altitude (13,000 m)	74.01	116.45

According to the ventilation resistance and ventilation pressure, the flow rate can be calculated under different working conditions as shown in Table 8. From the table, it can be seen that the air flow generated by forced ventilation is not affected by the ambient temperature because the pressure and resistance are both proportional to γ, while the flow rate is exactly equal to the square root of pressure divided by resistance, so it is not affected by γ.

Table 8. Flow rates under different operating conditions (unit: m^3/s).

	High Temperature (70 °C)	Low Temperature (−55 °C)
Sea level (0 m)	0.32	0.32
High altitude (13,000 m)	0.45	0.45

Based on the previous analysis, the airflow at sea level is the smallest, meanwhile the specific heat capacity of air is large and the heat dissipation ability of the airflow is better. Therefore, the winding temperature needs to be checked under high temperature conditions at high flight altitude.

The cooling flow rate obtained from Table 8 was input into MotorCAD software to calculate the winding temperature of the generator, and the results were obtained in Figure 11. The maximum temperature of the armature winding is 142.6 °C and the value of the excitation winding is 165.8 °C, both are under the pre-taken value of 180 °C and meet the operation requirements of the C-Class winding.

(**a**) (**b**)
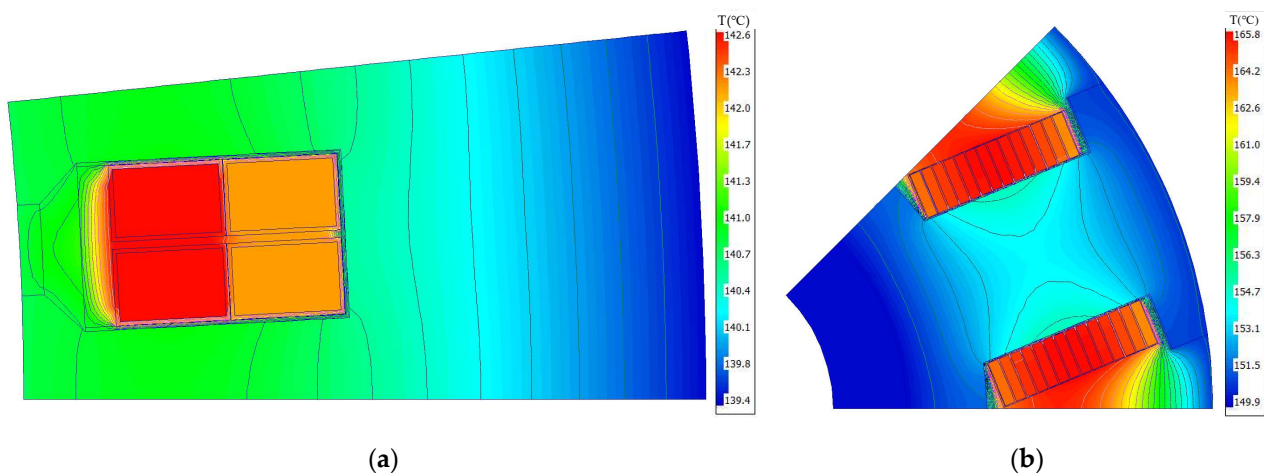
Figure 11. Generator temperature distribution during forced air cooling: (**a**) The armature winding; (**b**) The excitation winding.

3.3. Structural Design

The structure of the BSG is shown in Figure 12, including the PMG stator/rotor assembly, exciter stator/rotor assembly, MG stator/rotor assembly, housing, front/rear end caps, bearings and drive shaft.
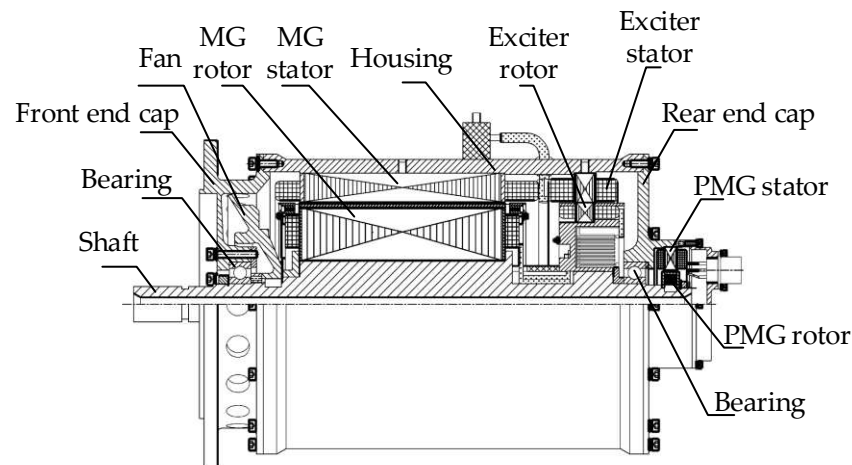
Figure 12. Generator structure diagram.

The rotor of a generator consists of four main parts: fan, MG rotor, exciter rotor and PMG rotor, as shown in Figure 13. The MG rotor includes the rotor core, excitation winding, damping winding, slot wedge and hoop ring, the exciter rotor includes the rotor core, armature winding, bracket, shield, rotating rectifier and heat sink and the PMG rotor includes the rotor core, permanent magnet and shield.
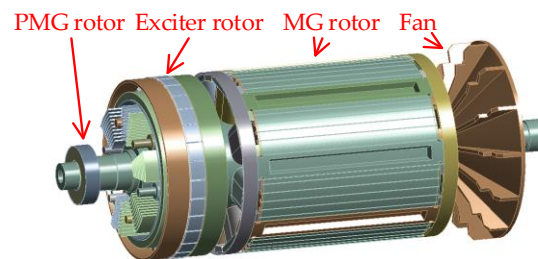

Figure 13. Generator rotor structure model.

Variety of materials are used for the generator rotor, corresponding to different components, and their physical properties are shown in Table 9.

Table 9. Physical properties of the rotor materials.

Materials	Density /(kg/m^3)	Young's Modulus /GPa	Poisson's Ratio	Yield Strength /MPa	Application Components
Pure copper	8890	117.7	0.35	315	Winding
Aluminum alloy	2780	68	0.33	325	Brackets
Electrical steel	7750	200	0.27	425	Iron core
Permanent magnets	8400	120	0.24	510	PMG rotor
Alloy steel	7740	119	0.32	1630	Shaft
Carbon Steel	7850	198	0.30	335	Iron core
Titanium alloy	4440	110	0.34	860	Sheathing
Laminate	2200	38.1	0.4	20	Insulated end plates

The rotor of the BSG has a complex structure and many materials, its stress cannot be simply calculated by the formula, but needs to be checked with the help of FEM simulation.

After inputting the rotor structure model and the corresponding material data into the simulation software, the obtained generator rotor mesh dissection model is shown in Figure 14.
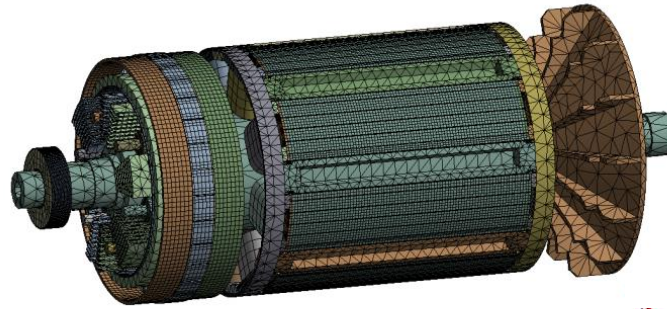

Figure 14. Generator rotor mesh sectioning model.

The rotor speed is set to 10,000 rpm, the equivalent stress distribution of the BSG rotor is obtained in Figure 15. The result shows that, the maximum value of the rotor stress is 361.56 MPa, which is located at the main generator rotor hoop ring.
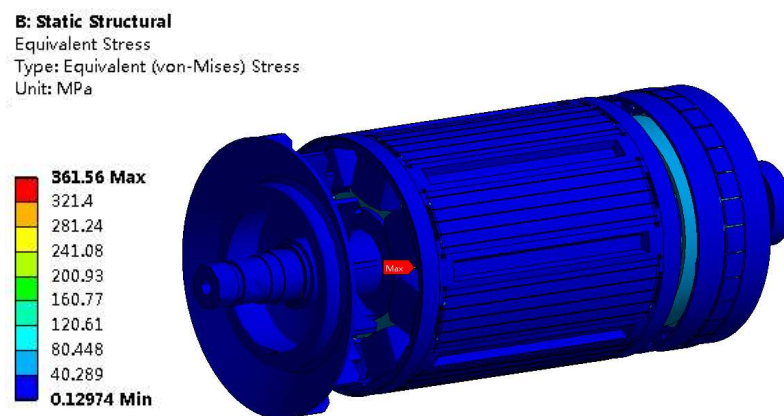

Figure 15. The equivalent stress distribution of the generator rotor.

After the above simulation verification, the stresses on the generator rotor are less than the yield strength of the relevant materials, so the rotor structure meets the mechanical requirements.

4. Experiments

A variable frequency BSG is developed based on the previous design results, as shown in the Figure 16. The generator contains three electrical interfaces: the MG electrical interface, the exciter electrical interface and the PMG electrical interface, which correspond to the stator windings of each stage of the generator, and the exciter electrical interface is responsible for the outputs of J-type thermocouples buried inside the generator.
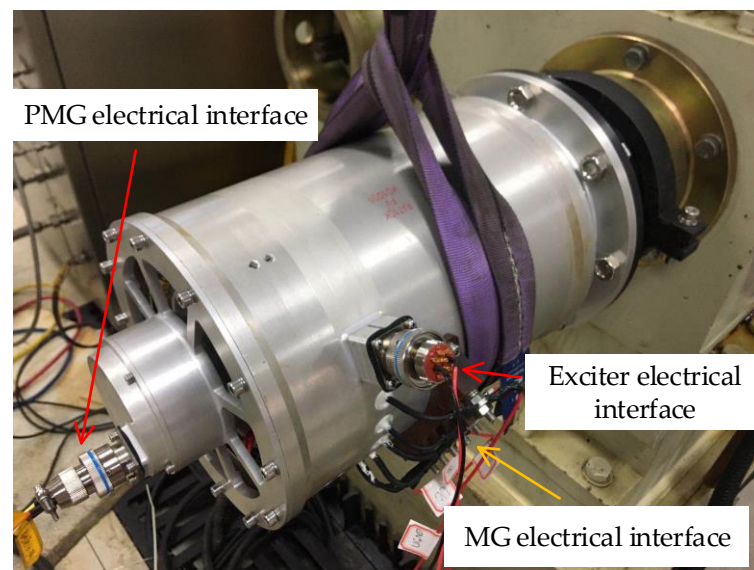
Figure 16. Prototype generator.

The architecture of the power generation system test platform is shown in the Figure 17, where MG_A, MG_B, MG_C and MG_N are the load voltage sampling signals, IF_+ and IF_− are the excitation windings of the exciter, TEMP1, TEMP2 and TEMP3 are the voltage signals of J-type thermocouples, PMG_A, PMG_B and PMG_C are the three phase armature windings of the PMG. The upper computer and the Generator Control Unit (GCU) are placed in an isolated room behind the wall to ensure the safety of the experimental personnel during the experimental operation. The generator is connected to the test-bed through an adapter plate and a shift sleeve, the output shaft speed of the test-bed can be controlled by the upper computer to drive the generator. The electrical interface of the MG is connected to the load bank, the voltage sampling line is connected to the GCU at the end of the load bank, and the electrical interfaces of the exciter and PMG are also connected to the GCU to realize the closed-loop control of the load voltages.
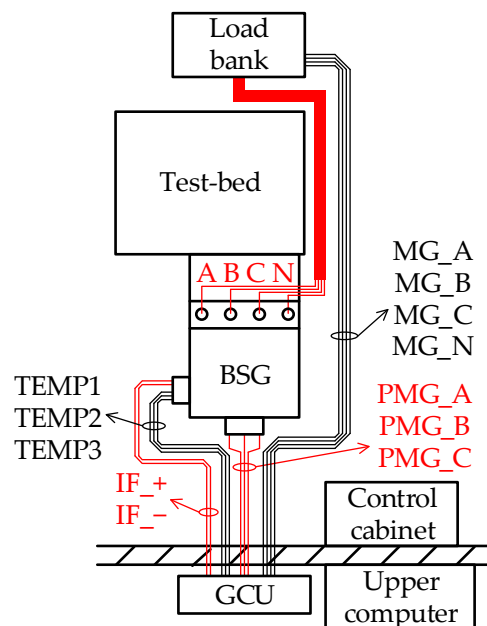

Figure 17. Schematic diagram of power generation system test platform.

Due to the short cable during the experimental test, the effect of its voltage drop can be almost ignored, so the rated output voltage of the generator is set to 235 V instead of 230 V in the experiment. The no-load characteristic of the generator at 6795 rpm is shown in Figure 18. Figure 18 shows that the results between experiment and FEM simulation are very close, so the FEM simulation applied in Section 3 is reliable. The saturation coefficient of the generator can be calculated from the no-load characteristic data, and the result is 1.03.
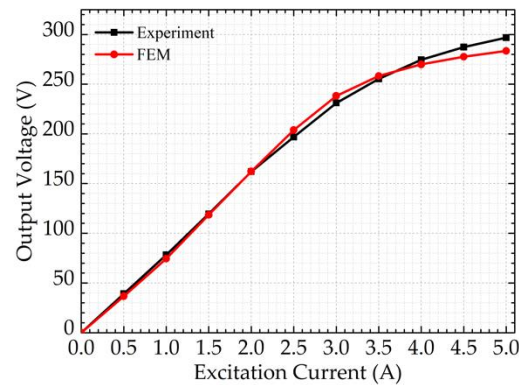

Figure 18. No-load characteristic of the BSG.

The external characteristics of the generator mean the variation of generator output voltage with load current at a certain speed, a certain excitation current and a certain power factor. The external characteristics curves of the BSG obtained from the experiment are shown in Figure 19. According to the data in the figure, the voltage regulation rate of the generator connected to inductive load and resistive load are 6.8% and 2.4%, respectively, at 6795 rpm; when the speed is increased to 9615 rpm, the voltage regulation rates under these two load conditions rise to 24.9% and 7.0%, respectively. This shows that the external characteristics of the BSG are softer at higher frequency.
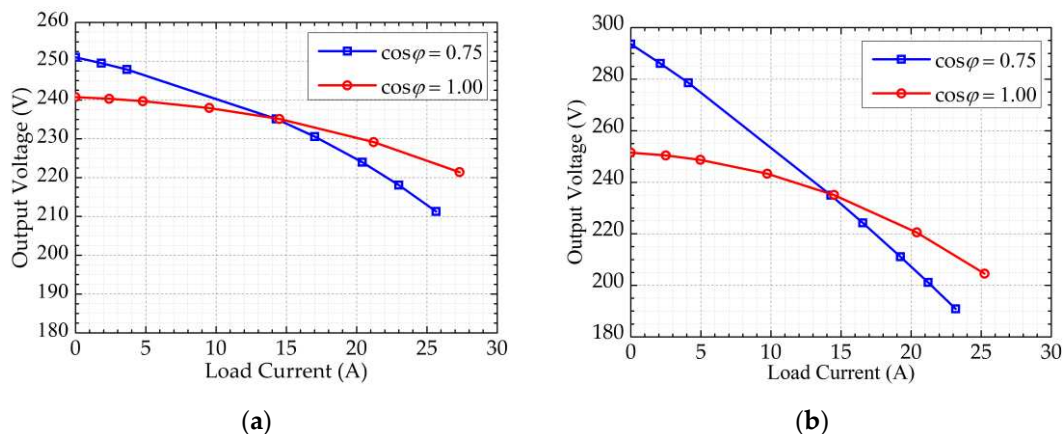

(**a**)　　　　　　　　　　　　　　　　　　(**b**)

Figure 19. External characteristics of the BSG: (**a**) External characteristics at 6795 rpm; (**b**) External characteristics at 9615 rpm.

The steady-state test data of the generator are shown in Table 10. These data show that the generator can operate normally from 6795 rpm to 9615 rpm, no load to overload and inductive load to resistive load.

Table 10. Generator steady-state test data.

Rotor Speed /rpm	Load Conditions	Excitation Voltage /V	Excitation Current /A	Output Voltage /V	Output Current /A
6795	No load	3.1	2.98	234.9	0
	100% load, cos φ = 0.75	3.7	3.54	235.0	14.3
	200% load, cos φ = 0.75	4.4	4.18	235.1	28.6
	100% load, cos φ = 1.00	3.3	3.14	235.0	14.4
	200% load, cos φ = 1.00	3.7	3.46	235.0	29.0
9615	No load	2.0	1.95	235.1	0
	100% load, cos φ = 0.75	2.6	2.44	235.0	14.3
	200% load, cos φ = 0.75	3.2	3.01	235.0	28.6
	100% load, cos φ = 1.00	2.2	2.08	235.1	14.5
	200% load, cos φ = 1.00	2.6	2.39	235.0	29.0

The harmonic data of the generator at different speeds and load conditions are shown in Table 11. Since the MG armature winding adopts 120° phase belt with 5/6 short pitch, which weakens the 3rd and 5th harmonic. As a result, the 7th harmonic is the highest content among all harmonics. MIL-STD-704F requires that the single harmonic content of the output voltage should not exceed 1.5% and the total harmonic content should not exceed 3.0%. From the data in Table 11, it can be seen that this designed BSG meets the requirement under full working condition.

Table 11. Harmonic data of the BSG under different load conditions.

Rotor Speed /rpm	Load Conditions	7th Harmonic	Total Harmonic
6795	No load	1.21%	2.21%
	50% load, cos φ = 0.75	1.19%	1.88%
	100% load, cos φ = 0.75	1.04%	1.66%
	150% load, cos φ = 0.75	0.99%	1.43%
	200% load, cos φ = 0.75	0.97%	1.46%
	50% load, cos φ = 1.00	1.00%	1.70%
	100% load, cos φ = 1.00	1.08%	1.66%
	150% load, cos φ = 1.00	0.94%	1.48%
	200% load, cos φ = 1.00	0.97%	1.46%
7500	No load	1.17%	1.99%
	50% load, cos φ = 0.75	1.06%	1.61%
	100% load, cos φ = 0.75	1.04%	1.47%
	150% load, cos φ = 0.75	1.00%	1.43%
	200% load, cos φ = 0.75	0.97%	1.46%
	50% load, cos φ = 1.00	1.05%	1.63%
	100% load, cos φ = 1.00	1.03%	1.54%
	150% load, cos φ = 1.00	0.99%	1.45%
	200% load, cos φ = 1.00	1.00%	1.60%

Table 11. *Cont.*

Rotor Speed /rpm	Load Conditions	7th Harmonic	Total Harmonic
9615	No load	1.34%	1.96%
	50% load, cos φ = 0.75	1.38%	1.92%
	100% load, cos φ = 0.75	1.32%	1.83%
	150% load, cos φ = 0.75	1.26%	1.92%
	200% load, cos φ = 0.75	1.22%	1.91%
	50% load, cos φ = 1.00	1.30%	1.91%
	100% load, cos φ = 1.00	1.19%	1.89%
	150% load, cos φ = 1.00	1.14%	1.84%
	200% load, cos φ = 1.00	1.10%	1.68%

5. Conclusions

This paper analyzes the performance requirements and operating conditions of the variable frequency BSGs, summarizes the influence of different operating conditions on the generator performances.

Based on the system characteristics and operating conditions, this paper proposes a corresponding design method that uses a multi-physical field design process including electromagnetic, fluid, temperature and stress fields.

In the electromagnetic design, this paper studies and analyzes the effects of generator air gap shape, damped winding structure and armature winding turns on generator harmonic content and negative sequence impedance, provides a reference basis for the optimal design of its power quality.

This paper analyzes the design of cooling duct characteristics such as air resistance and flow rate for the generator under forced-air cooling conditions, and calculates the MG winding temperature by temperature FEM simulation.

The overall structure of the generator is designed and the rotor stress is calculated to verify that the structural strength is enough to cope with the overspeed in the design requirements.

Finally, based on the previous analysis and design results, a prototype generator is manufactured and tested. The results show that the design method proposed in this paper can meet the requirements of the BSG under variable frequency operating conditions.

Institutional Review Board Statement: Not applicable.

Informed Consent Statement: Not applicable.

Data Availability Statement: Not applicable.

Conflicts of Interest: The authors declare no conflict of interest.

References

1. Wheeler, P.; Bozhko, S. The More Electric Aircraft: Technology and challenges. *IEEE Electrif. Mag.* **2014**, *2*, 6–12. [CrossRef]
2. Sarlioglu, B.; Morris, C.T. More Electric Aircraft: Review, Challenges, and Opportunities for Commercial Transport Aircraft. *IEEE Trans. Transp. Electrif.* **2015**, *1*, 54–64. [CrossRef]
3. Tom, L.; Khowja, M.; Vakil, G.; Gerada, C. Commercial Aircraft Electrification—Current State and Future Scope. *Energies* **2021**, *14*, 8381. [CrossRef]

4. Madonna, V.; Giangrande, P.; Galea, M. Electrical Power Generation in Aircraft: Review, Challenges, and Opportunities. *IEEE Trans. Transp. Electrif.* **2018**, *4*, 646–659. [CrossRef]
5. Burns, J.V. *Constant Speed Generating Systems*; SAE Technical Paper 771001; SAE: Warrendale, PA, USA, 1977. [CrossRef]
6. Barzkar, A.; Ghassemi, M. Electric Power Systems in More and All Electric Aircraft: A Review. *IEEE Access* **2020**, *8*, 169314–169332. [CrossRef]
7. Nøland, J.K.; Leandro, M.; Suul, J.A.; Molinas, M. High-Power Machines and Starter-Generator Topologies for More Electric Aircraft: A Technology Outlook. *IEEE Access* **2020**, *8*, 130104–130123. [CrossRef]
8. Wang, Y.; Nuzzo, S.; Zhang, H.; Zhao, W.; Gerada, C.; Galea, M. Challenges and Opportunities for Wound Field Synchronous Generators in Future More Electric Aircraft. *IEEE Trans. Transp. Electrif.* **2020**, *6*, 1466–1477. [CrossRef]
9. Pasquinelli, M.G.; Bolognesi, P.; Guiducci, A.; Nuzzo, S.; Galea, M. Design of a High-Speed Wound-Field Synchronous Generator for the More Electric Aircraft. In Proceedings of the 2021 IEEE Workshop on Electrical Machines Design, Control and Diagnosis (WEMDCD), Modena, Italy, 8–9 April 2021; pp. 64–69.
10. Wang, Y.; Wang, H.; Liu, W.; Wang, Q. A Novel Fuzzy PI Control Method for Variable Frequency Brushless Synchronous Generators. *Energies* **2021**, *14*, 7950. [CrossRef]
11. Zhao, X.; Wang, S.; Niu, S.; Fu, W.; Zhang, X. A Novel High-Order-Harmonic Winding Design Method for Vernier Reluctance Machine with DC Coils across Two Stator Teeth. *IEEE Trans. Ind. Electron.* **2022**, *69*, 7696–7707. [CrossRef]
12. Zhao, X.; Niu, S.; Zhang, X.; Fu, W. Flux-Modulated Relieving-DC-Saturation Hybrid Reluctance Machine With Synthetic Slot-PM Excitation for Electric Vehicle In-Wheel Propulsion. *IEEE Trans. Ind. Electron.* **2021**, *68*, 6075–6086. [CrossRef]
13. Camarano, T.; Wu, T.; Rodriguez, S.; Zumberge, J.; Wolff, M. Design and modeling of a five-phase aircraft synchronous generator with high power density. In Proceedings of the 2012 IEEE Energy Conversion Congress and Exposition (ECCE), Raleigh, NC, USA, 15–20 September 2012; pp. 1878–1885.
14. Jordan, S. *Multiphase Synchronous Generators for DC Aircraft Power Systems*; The University of Manchester: Ann Arbor, MI, USA, 2013.
15. Alnajjar, M.; Gerling, D. Six-phase electrically excited synchronous generator for More Electric Aircraft. In Proceedings of the 2016 International Symposium on Power Electronics, Electrical Drives, Automation and Motion (SPEEDAM), Capri, Italy, 22–24 June 2016; pp. 7–13.
16. Zhang, X. *Multiphase Synchronous Generator-Rectifier System for More-Electric Transport Applications*; The University of Manchester: Ann Arbor, MI, USA, 2019.
17. Iden, S.M.; Yost, K.; Spakovsky, M.V.; Allison, D.L. Conceptual Design Methods for New Aircraft Generators. In Proceedings of the 18th AIAA/ISSMO Multidisciplinary Analysis and Optimization Conference, Denver, CO, USA, 5–9 June 2017.
18. Wang, Y.; Nuzzo, S.; Gerada, C.; Zhao, W.; Zhang, H.; Galea, M. 3D Lumped Parameter Thermal Network for Wound-Field Synchronous Generators. In Proceedings of the 2021 IEEE Workshop on Electrical Machines Design, Control and Diagnosis (WEMDCD), Modena, Italy, 8–9 April 2021; pp. 5–9.
19. Nøland, J.K.; Nuzzo, S.; Tessarolo, A.; Alves, E.F. Excitation System Technologies for Wound-Field Synchronous Machines: Survey of Solutions and Evolving Trends. *IEEE Access* **2019**, *7*, 109699–109718. [CrossRef]
20. Bazzo, T.d.M.; Kölzer, J.F.; Carlson, R.; Wurtz, F.; Gerbaud, L. Multiphysics Design Optimization of a Permanent Magnet Synchronous Generator. *IEEE Trans. Ind. Electron.* **2017**, *64*, 9815–9823. [CrossRef]
21. Pyrhonen, J.; Jokinen, T.; Hrabovcova, V. *Design of Rotating Electrical Machines (2)*; John Wiley & Sons: Hoboken, NJ, USA, 2013.
22. Li, J.; Zhang, Z.; Lu, J.; Chen, C. Analysis and Design of Damper Winding of Salient-Pole Synchronous Generator for Negative-Sequence Reactance Reduction. In Proceedings of the 2018 21st International Conference on Electrical Machines and Systems (ICEMS), Jeju, Korea, 7–10 October 2018; pp. 543–548.
23. Fratila, M.; Benabou, A.; Tounzi, A.; Dessoude, M. Iron Loss Calculation in a Synchronous Generator Using Finite Element Analysis. *IEEE Trans. Energy Convers.* **2017**, *32*, 640–648. [CrossRef]
24. Wrobel, R.; Mellor, P.H.; Popescu, M.; Staton, D.A. Power Loss Analysis in Thermal Design of Permanent-Magnet Machines—A Review. *IEEE Trans. Ind. Appl.* **2016**, *52*, 1359–1368. [CrossRef]
25. Traxler-Samek, G.; Zickermann, R.; Schwery, A. Cooling Airflow, A. Losses, and Temperatures in Large Air-Cooled Synchronous Machines. *IEEE Trans. Ind. Electron.* **2020**, *57*, 172–180. [CrossRef]